2013 IEEE International Conference on Robotics and Automation (ICRA)
Karlsruhe, Germany, May 6-10, 2013

Can Concentric Tube Robots Follow The Leader?

Hunter B. Gilbert, *Student Member, IEEE*, and Robert J. Webster III, *Member, IEEE*

***Abstract*— Continuum robots have opened a broad array of applications to robotics in general, and the concentric tube continuum robots promise many benefits in medicine. Many people intuitively assume that these robots can deploy along a curved trajectory, in such a way that the curved shape of the robot's shaft remains unchanged as the tip progresses forward (i.e. "follow-the-leader" deployment). This capability would be useful in advancing along winding lumens (e.g. blood vessels, lung bronchi, etc.), as well as when the device is embedded in soft tissue and used as a steerable needle. However, in this paper we show that deploying in a follow-the-leader manner is not possible except in very special cases of tube precurvatures, combined with specific deployment sequences. We also show that follow-the-leader deployment is not possible even for many of the "simple" cases where one might intuitively expect it to be. Fortunately, useful special cases of perfect follow-the-leader behavior do exist, and we provide examples and describe the conditions that must be satisfied for this to be possible. We also study approximate follow-the-leader behavior, proposing a metric to quantify the similarity of a general deployment to a follow-the-leader deployment.**

I. Introduction

The desire to avoid critical structures and reach previously unreachable targets during needle biopsy and needle-delivered therapy has spurred the development of many kinds of steerable needles. Designs include bevel-tipped needles [1], needles with a pre-bent tip [2], and needles that extend a curved stylet [3], among others. For reviews, see [2], [4]. Early motivations for developing concentric tube continuum robots (also called "active cannulas" due to their usefulness in medicine, see Fig. 1), were (1) to generalize the steerability of steerable needles beyond soft tissues, to air or liquid filled cavities, and (2) to use this dexterity to create needle-diameter tentacle-like robot manipulators [5], [6]. While a great deal of the recent research in concentric tube robots has focused on the latter of these two motivations (see e.g. [7], [8]), efforts have also been made to address the former through motion planning (choosing actuator sequences to keep the shaft of the robot within anatomical bounds during deployment [9]), and in using a special case involving one curved tube and two straight tubes to hit targets in soft tissues [10], [11].

In the lung application of [12], for example, it would clearly be advantageous for the concentric tube robot to deploy in such a way that the shaft exactly follows the path through space traced by the tip of the device, i.e. a "follow the leader" deployment sequence [13]. This type of behavior was previously proposed for endoscope deployment by Ikuta et al. under the name "shift control" [14] and has been used to great advantage with other highly articulated surgical robots [15].

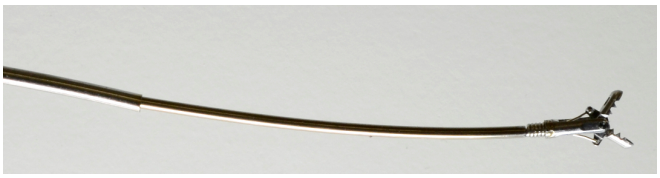

Fig. 1: A close-up of an active cannula robot with gripper.

In soft tissues, a benefit of using concentric tube robots is that they rely on internal forces rather than tip-tissue forces to bend [10]. In contrast, the properties of bevel-steered needles (shaft stiffness, tip design, etc.) must be matched exactly to tissue properties to achieve appreciable curvature, and coping with the sensitivity of the needle's behavior to small changes in tissue properties is one of the major current challenges needle steering research (see [2] and references therein). Thus, both deployment through open cavities and through soft tissues motivate the question we seek to answer in this paper: Can concentric tube robots deploy in a follow-the-leader manner?

Many people intuitively assume that the answer to this question is yes. And indeed, much of the initial motion planning and computational design work for concentric tube robots used approximations in mechanics-based models that make this true. For example, the simplest possible motion planning/design problem for active cannulas (involving tangent circular arcs) can be posed if tube interaction is totally neglected, and one assumes that every outer tube is infinitely stiff compared to all within it [16], [17]. As one adds bending effects into a planning or design problem [18], as well as bending plus transmission torsion effects [12], the computational intensiveness of the design or motion planning problem increases. Yet follow-the-leader deployment is still theoretically possible, given the approximate models employed.

However, experiments have shown that torsion in the curved sections of the robot can also dramatically affect robot tip positions in physical robots [19]. The equilibrium curve of two concentric, initially circularly precurved tubes is in general non-circular [20]. The complexity of the equilibrium curve even for this very special and seemingly simple case raises questions as to whether follow-the-leader deployment

This material is based upon work supported by the National Science Foundation under CAREER award IIS-1054331 and Graduate Research Fellowship DGE-0909667. Any opinions, findings, and conclusions or recommendations expressed in this material are those of the authors and do not necessarily reflect the views of the National Science Foundation.

The authors are members of the Mechanical Engineering department at at Vanderbilt University, and the Vanderbilt Initiative in Surgery and Engineering, Nashville, TN 37235, USA (e-mail: {hunter.b.gilbert, robert.webster}@vanderbilt.edu).

is possible at all for physical robots. Based on this, recent motion planning [9] and design [21] results have used the latest mechanics-based models [5], [6], which account for bending and torsion everywhere in the device, despite formidable computational challenges in doing so. These motion planning results have revealed that curvatures and actuation sequences must be very carefully selected to enable the robot to deploy through tubular anatomical constraints (i.e. in an approximate follow-the leader manner) [21].

In this paper we seek exact mathematical solutions to the follow-the-leader deployment problem. To accomplish this, we explore special cases of tube precurvatures and actuation sequences that enable follow-the-leader deployment. We begin in Section II by providing a mathematical definition for follow-the-leader behavior. Then, after reviewing the mechanics-based model for concentric tube robots in Section III, we proceed in Section IV to determine conditions that must be satisfied for pure follow-the-leader deployment. We show in Section V that these conditions imply that even a simple concentric tube robot with only two tubes, both of which are circularly precurved, can only exactly follow the leader when both lie in the same plane. We also describe a potentially useful special case involving helical precurvatures that can follow the leader exactly during deployment. In Section VI, we turn our attention to approximate follow-the-leader behavior, defining a metric for the closeness of a general deployment to a follow-the-leader deployment, and using it to investigate the effect of various tube design parameters and configuration variables on the ability of example concentric tube robots to follow the leader.

II. Follow-The-Leader Insertion

Before we can explore special cases and approximations of follow-the-leader behavior, it is useful to have a mathematical definition that describes deployment along a single trajectory. We denote the spatial configuration of the robot by a time-varying, arc-length parameterized transformation $\boldsymbol{g}(s,t) \in SE(3)$ which assigns a position $\boldsymbol{p}(s,t) \in \mathbb{R}^3$ and orientation $\boldsymbol{R}(s,t) \in SO(3)$ to each arc length $s \in [0, L(t)]$. The function $L(t)$ represents the exposed length of the robot, which increases during a deployment, and hence is a function of time. The differential kinematic equations describing the evolution of the transformation are given as $\boldsymbol{g}' = \boldsymbol{g}\widehat{\boldsymbol{\xi}}$, where $\boldsymbol{\xi} \in \mathbb{R}^6$ contains the body frame twist coordinates $\boldsymbol{\xi} = \begin{bmatrix}\boldsymbol{v}^T & \boldsymbol{u}^T\end{bmatrix}^T$ and the prime denotes the derivative with respect to s. The $\widehat{\ }$ denotes conversion of the vector in $\mathbb{R}^6$ to an element of the Lie algebra $\mathfrak{se}(3)$. The vector $\boldsymbol{u}$ may be thought of as the curvature or "angular velocity" (with respect to arc length) of the frame, and $\boldsymbol{v}$ as the "linear velocity" (with respect to arc length) of the frame $\boldsymbol{g}$. We assume that the $\boldsymbol{z}$ axis of $\boldsymbol{R}$ is tangent to the curve, and the transformation propagates with unit velocity[1], meaning that $\boldsymbol{v} = \begin{bmatrix}0 & 0 & 1\end{bmatrix}^T$. Equivalently, the components of the transformation $\boldsymbol{g}$ can be expressed as

$$\begin{aligned}\boldsymbol{R}'(s) &= \boldsymbol{R}(s)[\boldsymbol{u}(s)]_\times \\ \boldsymbol{p}'(s) &= \boldsymbol{z}(s)\end{aligned} \tag{1}$$

where we also assume initial conditions $\boldsymbol{R}(0) = \boldsymbol{R}_{\boldsymbol{z}}(\psi)$ (a rotation about the $\boldsymbol{z}$-axis by ψ), and $\boldsymbol{p}(0) = \boldsymbol{0}$. The operation $[\cdot]_\times$ is the isomorphism between a vector in $\mathbb{R}^3$ and its skew-symmetric cross product matrix.

For follow-the-leader deployment, the rotation matrix is unimportant except as it affects $\boldsymbol{p}(s)$. To achieve follow-the-leader deployment, the function $\boldsymbol{p}(s)$, which is the solution to (1), must remain the same for any two actuator values in the deployment sequence. There is a mathematical subtlety here: for two different solutions, the domain of s may be different. To resolve this ambiguity, we can require that the two solutions be the same over the length of the "shorter" solution. As we will see shortly, however, a differential approach will allow us to avoid this issue altogether.

The definite integral which gives the solution to the positional part of (1) is

$$\boldsymbol{p}(s) = \int_0^s \boldsymbol{z}(\sigma)d\sigma. \tag{2}$$

The actuator values $\boldsymbol{q}(t)$ are changing in time during a deployment, so we require that at any given time $\dot{\boldsymbol{p}}(s) = 0$ for $s \in [0, L]$. By the fact that the limits of the integral are not time dependent, the time derivative may be commuted with the integration to give

$$\dot{\boldsymbol{p}} = \int_0^s \dot{\boldsymbol{z}}(\sigma)d\sigma = \boldsymbol{0} \tag{3}$$

Since this must hold for every valid s, we define a follow-the-leader deployment as one for which

$$\dot{\boldsymbol{z}}(s) = \boldsymbol{0}. \tag{4}$$

We already know that $\dot{\boldsymbol{z}}(0) = \boldsymbol{0}$ from the initial conditions of (1). Noting that (1) is differentiable in time except at perhaps a finite number of points s_i where $\boldsymbol{u}(s_i)$ may change discontinuously at the tube endpoints, it is necessary and sufficient that $\dot{\boldsymbol{z}}'(s) = \boldsymbol{0}$. From (1), we obtain

$$\dot{\boldsymbol{z}}' = \dot{u}_y\boldsymbol{x} + u_y\dot{\boldsymbol{x}} - \dot{u}_x\boldsymbol{y} - u_x\dot{\boldsymbol{y}} = \boldsymbol{0}. \tag{5}$$

Before going further, we note that the time derivatives of the unit vectors in $\boldsymbol{R}$ are constrained also by a kinematic relation like (1), which is that $\boldsymbol{R}^T\dot{\boldsymbol{R}} = [\boldsymbol{\omega}]_\times$ for a vector $\boldsymbol{\omega}$ which represents the body frame angular velocity (in time rather than arc length). From this condition, we may deduce that as a result of (4), ω_x and ω_y must both be zero, and that $\boldsymbol{x}\cdot\dot{\boldsymbol{y}} = -\omega_z$ and $\dot{\boldsymbol{x}}\cdot\boldsymbol{y} = \omega_z$. Taking the dot product of (5) with the three vectors $\boldsymbol{x}$, $\boldsymbol{y}$, and $\boldsymbol{z}$ will still result in the same three constraints as the original equations but along different directions. The dot product with $\boldsymbol{z}$ is trivially zero as a result of our definition of follow-the-leader behavior, but the other two dot products reveal two scalar differential constraint equations that must be satisfied. In matrix form, these are:

$$\frac{d}{dt}\begin{bmatrix}u_x \\ u_y\end{bmatrix} = \begin{bmatrix}0 & \omega_z \\ -\omega_z & 0\end{bmatrix}\begin{bmatrix}u_x \\ u_y\end{bmatrix}. \tag{6}$$

[1]This corresponds to assuming that the material of which our robot is made undergoes negligible shear and extension.

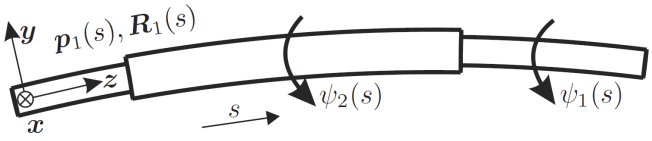

Fig. 2: A diagram of a section of two concentric tubes showing relevant variables. The position and orientation are those of the innermost tube (tube 1), while each tube has its own angular displacement ψ. The tubes as illustrated here have a slight positive curvature about the x axis.

The interpretation of these constraints is that when the backbone frame rotates about the local $\boldsymbol{z}$-axis with angular velocity $+\omega_z$, the $\boldsymbol{x}$- and $\boldsymbol{y}$-curvatures defining the curve in (1) must rotate about the local $\boldsymbol{z}$-axis with angular velocity $-\omega_z$ in order to maintain the same space curve.

III. Mechanics-Based Model Review

The curvature vector $\boldsymbol{u}$ from the previous section is defined by a mechanics-based model that results in a set of differential equations which define a boundary value problem [5], [6], which is reviewed in this section. The curvature $\boldsymbol{u}_i = \begin{bmatrix} u_{ix} & u_{iy} & u_{iz} \end{bmatrix}^T$ of each tube is written in the material frame of the respective tube. Here $i \in 1, ..., N$ denotes the tube number with tube 1 having the smallest diameter. The precurved shape of each tube is expressed as a material-attached frame in the Frenet-Serret convention as $\boldsymbol{u}_i^*(s) = \begin{bmatrix} u_{ix}^*(s) & 0 & u_{iz}^*(s) \end{bmatrix}^T$, where we will refer to u_{ix}^* as the *curvature* and u_{iz}^* as the *torsion* of the frame. Let the variables $\psi_i(s)$ be the angular rotations of each tube, which may be thought of as the angular displacement about the local $\boldsymbol{z}$-axis between the material frame and the zero-torsion or rotation-minimizing Bishop frame which begins at $\boldsymbol{R}(0) = \boldsymbol{I}$. A diagram of the variables of interest is shown in Fig. 2. From this point forward, as in the previous section, for notational brevity, the explicit dependence on s will be suppressed except where not clear from context.

The multi-point boundary value problem for a concentric tube robot with no applied external loads is given in [22] as:

$$\begin{aligned} \psi_i' &= u_{iz} \\ u_{iz}' &= u_{iz}'^* + \frac{1}{EI}\frac{E_i I_i}{G_i J_i}\sum_{k=1}^{N} E_k I_k u_{ix}^* u_{kx}^* \sin\left(\psi_i - \psi_k\right) \end{aligned} \tag{7}$$

for $i = 1, ..., N$, with boundary conditions

$$\begin{aligned} \psi_i(0) &= \psi_{i0} \qquad && i = 1, ..., N \\ u_{iz}(\ell_i) &= u_{iz}^*(\ell_i) \qquad && i = 1, ..., N. \end{aligned} \tag{8}$$

Here $\psi_i(0)$ specifies the initial z-axis rotation of tube i which may be controlled by an actuator, and the latter boundary conditions on u_{iz} result from the fact that each tube must have zero torsional internal moment at its endpoint (i.e. at the arc length ℓ_i). We use a linear constitutive law for the internal moment, $\boldsymbol{m}_i = \boldsymbol{K}_i(\boldsymbol{u}_i - \boldsymbol{u}_i^*)$, where $\boldsymbol{K}_i$ is a stiffness matrix. Here $\boldsymbol{K} = \text{diag}(E_i I_i,\ E_i I_i,\ G_i J_i)$, E_i is Young's Modulus, and I_i is the area moment of inertia of the tube cross section, which is assumed to be annular, about the $\boldsymbol{x}$ or $\boldsymbol{y}$ axes. The term EI is the sum over all the stiffnesses, $EI = \sum_{k=1}^{N} E_k I_k$. Similarly, G_i is the shear modulus and J_i is the area moment of inertia about the tangent axis.

It is important to note that although the precurved shape of a tube cannot change during an insertion, the function $\boldsymbol{u}_i^*(s)$ which describes it may have a nonzero time derivative as a result of the tubes being translated by the actuators, which changes the correspondence between a physical tube and the assigned arc length s. In addition, it is important to realize that the sum is performed only over those tubes which exist at the arc length being evaluated, and that the equations are only valid for tube i over the length that it exists.

The boundary value problem determines the torsional behavior, but the local $\boldsymbol{xy}$-curvature is found in closed form as a weighted sum of the precurvatures rotated into the frame of tube 1,

$$\boldsymbol{u}_{xy} = \frac{1}{EI}\sum_{j=1}^{N} E_j I_j \begin{bmatrix} \cos(\psi_j - \psi_1) \\ \sin(\psi_j - \psi_1) \end{bmatrix} u_{jx}^*. \tag{9}$$

It is this frame which we define to be the central axis frame (i.e. the "backbone frame") of the robot. Thus, the final robot curve is found by integrating (1) with $\boldsymbol{u} = \begin{bmatrix} \boldsymbol{u}_{xy}^T & u_{1z} \end{bmatrix}^T$.

IV. Necessary and Sufficient Conditions for Follow-The-Leader Deployment

To determine conditions for concentric tube follow-the-leader deployment, we first assume a deployment sequence in which no tube which ends at an arc length $s < L$ undergoes insertion or retraction, and that all tubes which advance axially to extend the robot's tip do so together.[2] Continuing from (6), we can substitute in the robot model (9) and replace ω_z with $\dot{\psi}_1$ by definition of the backbone. After applying the chain and product rules and canceling terms, two constraint equations emerge:

$$\begin{aligned} &\sum_{j=1}^{N} E_j I_j \left[\cos\left(\psi_j - \psi_1\right) u_{jx}^* \dot{\psi}_j + \sin\left(\psi_j - \psi_1\right) \dot{u}_{jx}^*\right] = 0 \\ &\sum_{j=1}^{N} E_j I_j \left[\sin\left(\psi_j - \psi_1\right) u_{jx}^* \dot{\psi}_j - \cos\left(\psi_j - \psi_1\right) \dot{u}_{jx}^*\right] = 0. \end{aligned} \tag{10}$$

Note that all of the rotational configuration functions ψ_i appear in these conditions, as well as their time derivatives. The time derivatives of the precurvature functions also appear, and are nonzero for tubes that have non-constant precurvature and are undergoing insertion.

For a follow-the-leader insertion, the differential equations (10) must be consistent with the mechanics of the robot (7). Before attempting to find special cases of the various functions involved where this is true, we first examine the two-tube case.

[2]Note: assuming this deployment sequence is not very restrictive. It precludes from consideration only one trivial special case where the curvature of a tube that ends at $s < L$ has precisely the same curvature as the collection of tubes present at its tip have on either side (in arc length) of its tip. A simple example of this would be two tubes with equal curvatures that lie in the same plane. For these tubes, there is no tube interaction or deformation, and a tube that ended at $s < L$ could be moved axially without changing the net curve, since it matches both tubes' precurvatures.

V. The Two-Tube, Constant-Precurvature Case

A. Planar Constant Precurvatures

One prototype design which is appealingly simple is that of two tubes which have precurvatures that are constant in arc length and planar (i.e. precurvatures that are circular arcs). Since the tubes have constant precurvature, $u_{jx}'^{*} = \dot{u}_{jx}^{*} = 0$. The constraints (10) then simplify to

$$\begin{aligned} E_1 I_1 u_{1x}^{*} \dot{\psi}_1 + E_2 I_2 \cos(\psi_2 - \psi_1) u_{2x}^{*} \dot{\psi}_2 = 0 \\ E_2 I_2 \sin(\psi_2 - \psi_1) u_{2x}^{*} \dot{\psi}_2 = 0. \end{aligned} \tag{11}$$

From this we conclude that when both curvatures are nonzero, unless $\psi_2 - \psi_1 = n\pi$ for some integer $n \in \mathbb{Z}$, this system has only the trivial solution $\dot{\psi}_1 = \dot{\psi}_2 = 0$, meaning that the tubes cannot undergo rotation at any arc length. If $E_1 I_1 u_{1x}^{*} = E_2 I_2 u_{2x}^{*}$, then the solutions for odd n will be completely straight (as indicated by (9)), and, in these particular solutions, any rotation of the tubes with $\dot{\psi}_1 = \dot{\psi}_2$ would satisfy (11), corresponding to spinning the now straight collection of tubes about its axis.

Elaborating on the $\psi_2 - \psi_1 = n\pi$ condition, if it were not true, (11) would require the functions $\psi_1(s)$ and $\psi_2(s)$ to be constant in time. But they cannot be, because the robot is deploying and increasing in total arc length. This implies that the distal boundary conditions in (8) are moving in arc length. In this case, if u_{iz}' is nonzero at one of the distal boundaries, then $\dot{\psi}_i$ must be nonzero for at least some part of the overlapped tube length in order to maintain the distal boundary conditions. To see this, examine the total derivatives of the distal boundary constraints,

$$\left[\frac{\partial u_{iz}}{\partial s} \frac{dL}{dt} + \frac{\partial u_{iz}}{\partial t} \right]_{s=L} = 0. \tag{12}$$

From this equation, we see that if u_{iz}' is nonzero, then the fact that dL/dt is nonzero means that $\dot{u}_{iz} = \dot{\psi}_i'$ cannot be zero, implying also that somewhere in the neighborhood of $s = L$, $\dot{\psi}_i \neq 0$. Thus, it is never possible for two constant-curvature tubes to follow the leader exactly during deployment other than when $\psi_2 - \psi_1 = n\pi$ (i.e. when the tube curvatures lie in the same plane).

B. Helical Precurvatures

If either of the precurved shapes is a helix, then by the arguments in the previous subsection, $\psi_2 - \psi_1$ will not equal $n\pi$ everywhere unless additionally both tubes have the same helical torsion u_z^{*}. If they did not, $\psi_1'(L) = u_{1z}^{*}(L) \neq u_{2z}^{*}(L) = \psi_2'(L)$, which implies that $\psi_2 - \psi_1$ is not constant. Equal torsion in the Frenet-Serret sense is therefore a necessary condition for follow-the-leader deployment of two helical tubes.

C. Stability of Solutions

The odd and even solutions for n in the previous two subsections do represent different solutions. The odd solutions are only stable in a robot that does not have bifurcations (see [19] for further information on bifurcations) in the associated initial value problem of (7). For two tube, constant-curvature interactions, it has been shown in prior work [20] that bifurcations are avoided when the robot satisfies the nondimensional inequality:

$$\lambda = L^2 u_{1x}^{*} u_{2x}^{*} \frac{E_1 I_1 E_2 I_2 (G_1 J_1 + G_2 J_2)}{G_1 J_1 G_2 J_2 (E_1 I_1 + E_2 I_2)} < \frac{\pi^2}{4}. \tag{13}$$

It can be shown that this condition holds as long as both tubes have the same precurved torsion, though the original derivation assumed circular tubes. As λ approaches the critical value, the odd solutions become progressively "less stable" and so any designer wanting to leverage the odd solutions in a device designed to follow the leader would likely want to maintain some margin of safety below this critical value.

D. Summary of Follow-The-Leader Cases

Based on the discussions in preceding subsections, we can now describe some potentially useful cases where follow-the-leader behavior is possible for two tubes:

1) $\mathbf{u_{2x}^{*} = 0}$ or $\mathbf{u_{1x}^{*} = 0}$. In this case one but not both of the tubes has zero precurvature, meaning that the final shape consists of two tangent circular or helical arcs with different curvatures. This case was has been identified and elaborated upon previously for circular tubes (see e.g. [10]).
2) $\mathbf{u_{1z}^{*} = u_{2z}^{*} = 0}$. Both tubes are circular in precurvature and we ensure that $\psi_2 - \psi_1 = n\pi$. The final shape consists of two circular arcs (which may have different radii based on tube stiffnesses and precurvatures) that lie in the same plane, and are tangent to one another. For even n these two arcs will curve in the same direction, while for odd n, they may curve in the same or opposite directions.
3) $\mathbf{u_{1z}^{*} = u_{2z}^{*} \neq 0}$. Both tubes are helical in shape with the same helical torsion, but not necessarily the same curvature. The interaction results in a piecewise helical final shape as long as $\psi_2 - \psi_1 = n\pi$, where as mentioned previously, the even and odd solutions are different. The even solutions will always contain two helical segments which curve in the same direction and have equal torsion. The segments of the odd solutions may curve in the same or opposite directions.

It is interesting to note that in all of these cases, the follow-the-leader solutions are the ones which have no internal material torsion. This fact is evident from (7) since $\sin(\psi_i - \psi_k) = 0$ and therefore $u_{iz} = u_{iz}^{*}$ along the whole length of each tube.

E. Required Deployment Sequences

In each of the cases enumerated in the prior subsection, follow-the-leader insertion must begin with insertion of both tubes together (fully overlapping), followed by insertion of one tube only while holding the other fixed. These tubes will be called the "moving" and "fixed" tubes respectively for this stage of insertion. Since the moving tube has constant curvature, the interaction of the two tubes will remain unchanged as long as the actuation satisfies the requirement that $\psi_i(0)$ is fixed. If the moving tube has any precurved

torsion (in the Frenet-Serret frame sense), an actuator will have to rotate the tube base, which is at negative arc length, to maintain a constant angle at $s = 0$. If the fixed tube is moved at all after the moving tube has been extended, then the condition $\dot{u}^*_{ix} = 0$ has been violated and the sum EI is no longer constant at the discontinuity where the fixed tube ends, meaning that the assumptions required for (10) are no longer valid. The follow-the-leader behavior will cease in this case (unless the precurvatures are both aligned and equal to one another) meaning that the shaft of the robot will deviate from the path traced previously by its tip. For the same reason, a tube with a step change in curvature (e.g. a tube with an initial straight transmission followed by a circularly precurved tip section) will not be able to deploy in a follow-the-leader manner if the change in curvature occurs in the length from $s = 0$ to $s = L$.

F. The Space of Curves Enabled by Helical Precurvatures

The case of two helically precurved tubes provides a large family of follow-the-leader curves for the robot, even for only two tubes. For a visual aid, two final shapes for a single tube set are shown in Fig. 3b. Parameters that can be selected include the handedness of the helices (whether u^*_z is positive or negative), the curvature of each tube, the overlapped insertion arc length, the non overlapped insertion length of one tube extending beyond the overlapped section, and a rigid rotation of the entire final shape. In practical applications involving insertion through a winding tube or through soft tissue (as discussed in the Introduction), one could envision having many helical tubes pre-made, and allowing a planning algorithm to select the best pair of tubes, based on the target location and any relevant obstacles and tissue boundaries. Furthermore, the solutions will be easy to compute because the torsional mechanics do not need to be solved and the kinematics can be solved in closed form [19].

VI. Follow The Leader With General Tube Sets

In the general case where we cannot simplify the constraints further than (10), it is less clear for which special cases of precurvature follow-the-leader deployment will be possible. Certainly, any set of circularly precurved tubes could follow the leader if the angular displacement between every combination of two tubes is $n\pi$ for any integer n. This assumes that the insertion length is sufficiently short and the tubes have low enough curvatures that the initial value problem associated with (7) has not undergone a bifurcation. The solution would be planar and could have curvature that switches directions. By a similar argument, three helices with equal torsion could also follow the leader. However, general methods do not yet exist to predict bifurcations in sets of more than two tubes, making the design of such systems more challenging.

It is possible that other special case functions exist for which the constraints in (10) can be consistent with the torsional mechanics in (7) for more general solutions of ψ and more general, non-constant choices of precurvature. Identifying them (if they exist), and determining whether

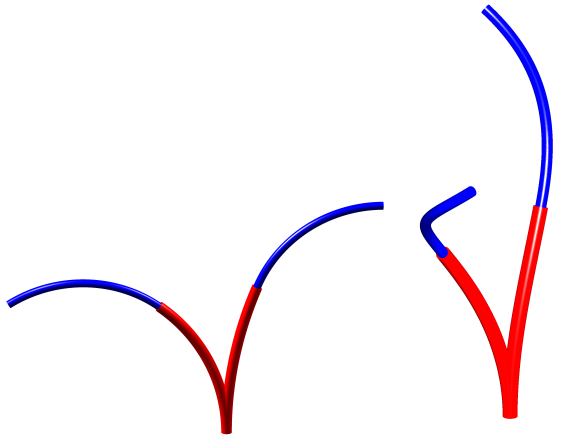

(a) Circular Tubes (b) Helical Tubes

Fig. 3: (a) Two circular tubes are shown. These tubes have an overall insertion length of 12 cm, with an overlapped tube length of 6 cm. The left solution has the tubes aligned, while the right solution has the inner tube rotated the opposite direction. (b) The same tube curvatures are used, but both tubes are given the same pre-curved torsion, resulting in two helical tubes. All of these configurations can be reached in a perfect follow-the-leader manner.

they are potentially useful in various applications remain open research questions. As with the special case solutions we have described in this paper, any new solutions will involve both specific precurvatures and specific deployment sequences, because the torsional dynamics are completely defined (i.e. the time derivatives of all ψ_i are determined completely by the mechanics model of the robot). Thus, the two additional constraints from Section IV are unlikely to be satisfied except in very special cases. Maintaining the constraints, which are infinite-dimensional, with only a finite number of actuator inputs is a challenging endeavor that will require assistance from special properties of the precurvature functions selected.

One potential way to solve this problem through design is to "key" the tubes together, which constrains their rotational motion with respect to one another. Effectively, this causes $\dot{\psi}_i = 0$ for constant-precurvature tube shapes at any initial angular displacement. One way that has been suggested to achieve this (though not physically prototyped to the best of the authors' knowledge) is to extrude tubes with a polygonal rather than annular cross section [23]. In this case, any number of constant-precurvature tubes can be made to follow the leader by using an insertion sequence similar to that described earlier for two tubes, namely one in which all tubes advance together initially, with one or more stopping sequentially at specified arc length points and then remaining stationary after stopping.

VII. Approximate Follow-The-Leader Deployment

In some cases, approximate follow-the-leader deployment may be sufficient to accomplish a given task. In order to measure closeness to exact follow-the-leader deployment, we define an error metric that quantifies the maximum

displacement at any arc length along the backbone. Our error metric is defined as

$$E = \max_{t_1} \max_{t_2} \max_{\tilde{s}} \|\boldsymbol{p}(\tilde{s}, t_1) - \boldsymbol{p}(\tilde{s}, t_2)\| \qquad (14)$$

where $\tilde{s}$ represents arc length over the length of the robot which exists for both times t_1 and t_2. That is, $\tilde{s} \in [0, \tilde{L}]$ with $\tilde{L} = \min(L(t_1), L(t_2))$. This error metric captures the largest movement of the backbone at any arc length point during the entire deployment period, and has units which are the same as $\boldsymbol{p}$. Minimizing this error over the set of possible actuator trajectories would give a best-case follow-the-leader behavior for a given robot design. This error metric could also provide a bound for planning and design algorithms which seek to design both the properties of the tube set and the actuation sequence to be used for a specific task.

We now apply this error metric to explore the case of two circularly precurved tubes whose curvatures do not lie in the same plane, which we previously showed cannot deploy in an exact follow-the-leader manner. To quantify the deviation from pure follow-the-leader behavior during deployment of these tubes, $\psi_1(0)$ and $\psi_2(0)$ are held fixed and then the two tubes are translated forward to a predetermined length. The maximum error E is computed according to (14) for a number of tube curvatures and choices of $\psi_2(0) - \psi_1(0)$ (see example case in Fig. 4).

To generate the data shown in the figure, the model equations (7) for ψ_i were solved via a nonlinear method of mean weighted residuals (MWR). The solution is assumed to be piecewise quadratic with 20 elements, which was determined to have sufficient accuracy by a convergence check showing that the error in ψ is on the order of 10^{-5} between the 20 element, 40 element, and 60 element solutions for a solution similar to the ones under consideration. MATLAB's `fsolve` was used to solve the MWR equations. After obtaining the solution for ψ_i, the kinematic equations (1) are integrated by the Dormand-Prince 5^{th} order Runge-Kutta pair and the solution interpolated to 1000 evenly spaced points along the length of that particular solution. To compute E, the solution for $\boldsymbol{p}$ is computed for 200 discrete steps of insertion, and each pair of unique solutions is checked by truncating and linearly interpolating the longer solution to the same arc-length points as the shorter solution, at which point the innermost maximum is evaluated. The maximum value is then found by brute-force search.

The results of this simulation for a few choices of tube curvature are shown in Fig. 4. Each of these insertions was carried out for a length of 10 cm for two tubes with stiffness $EI = 1$, which for the case of $u^*_{ix} = 12$ results in a bifurcation parameter of $\lambda = 1.87 < \pi^2/4$ using a Poisson's ratio of $\nu = 0.3$. Clearly, as the rotation between the tubes increases, the maximum follow-the-leader error increases until the angle becomes close to $180°$, where the error sharply decreases to zero. The reason for this is that in all of the situations tested, the tube curvatures and overlapped length are sufficiently low that no bifurcation is present in the system, and in this case we showed earlier that

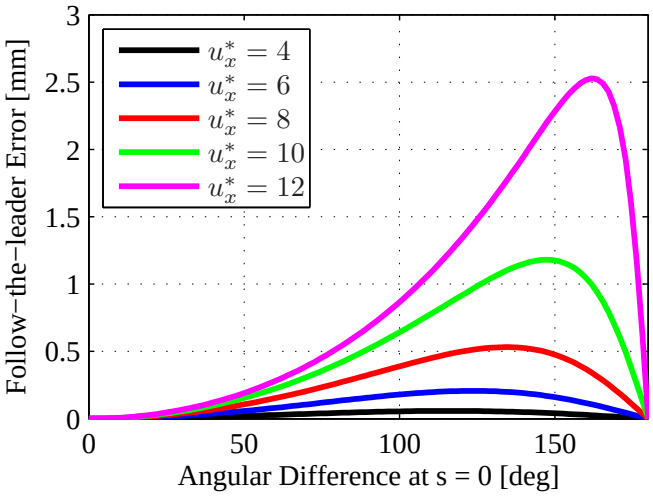

Fig. 4: The follow-the-leader error increases with increasing angular difference $\psi_2(0) - \psi_1(0)$ and with increasing curvature of the tube pair, but equals zero when the angular difference is $n\pi$ as expected.

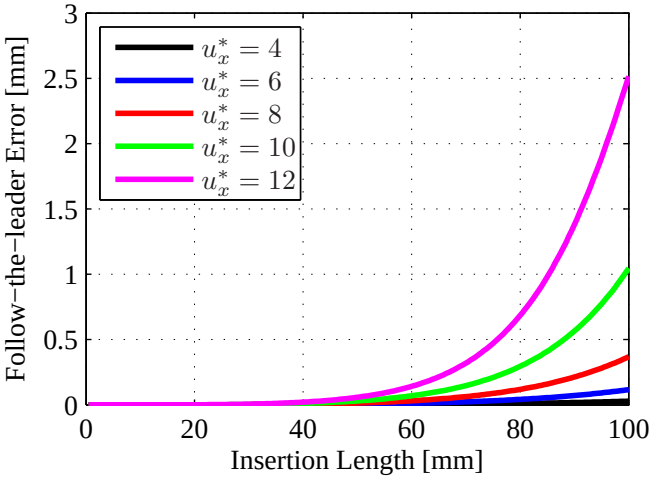

Fig. 5: The follow-the-leader error increases with increasing insertion length.

$\psi_2 - \psi_1 = \pi$ yields perfect follow-the-leader behavior. In this particular scenario, the error will also grow monotonically with insertion length, which is evident from the fact that at zero length the error must be zero, while any finite length encompasses the same insertion as all shorter lengths. This effect is clearly displayed in Fig. 5, which shows the results of increasing insertion length for the same tube sets as before, with the angular difference set to 160 degrees at $s = 0$. These simulations illustrate that two circularly curved tubes with curvatures gradual enough to avoid bifurcations can approximate follow-the-leader behavior with deviations on the order of a few mm over a 10 cm insertion. Note that deviations will be greater for longer arc lengths and more aggressively curved tubes (the upper bounds on curvature to avoid self-damage to the device are significantly higher than those imposed by design for total bifurcation avoidance [19]).

VIII. Discussion and Conclusions

We have shown in this paper that while care must be taken in both precurvature selection and deployment sequence used, it is possible to deploy concentric tube robots in a follow-the-leader manner. We provided necessary and sufficient conditions for this to occur and studied specific cases where pure follow-the-leader deployment is achievable. We also explored approximate follow-the-leader behavior, quantifying the deviation of a general deployment from a pure follow-the-leader deployment and providing a metric for it that we believe will be useful in future design and motion planning research.

In terms of medical applications involving traversing open or liquid filled cavities, winding lumens, or passing through soft tissues, the particular case of two constant precurvature tubes fortunately provides a large design space of possible curves that includes both circular arcs and helical segments, among other curves. Thus, we believe that even this simple case will be useful for many medical applications where concentric tubes act as steerable needles in both soft tissues and open or liquid-filled spaces. It is also likely that some applications will be able to make use of concentric tubes that approximately follow the leader. In open lumens, there may be a margin of open space around the robot that can be used. In soft tissues, some mild stretching of the tissue can likely be permitted with no adverse effects to the patient.

There are at least two other practical, real-world effects that remain to be studied in future work on follow-the-leader deployment. First, the effects of tissue-robot interactions have yet to be investigated in this context. Fortunately, the mechanics-based model described in Section III can account for external loading, so it is possible to study how surrounding tissue will affect the cannula, if the interaction forces between the two can be measured or predicted. Second, the model in Section III does not include friction, and the implications of the hysteresis induced by friction [24] remain to be studied in context of follow-the-leader deployment.

One conclusion that can be drawn from the results in this paper is that, perhaps counter intuitively, the concentric tube robot prototypes built to date are typically incapable of pure follow-the-leader deployment. The strong constraints follow-the-leader deployment places on both precurvature functions and deployment sequences mean that concentric tube robots not specifically designed for follow-the-leader deployment are almost certainly incapable of it. The results in this paper, once experimentally vetted, appear poised to expand the set of curves achievable by concentric tube robots in applications where they are used as steerable needles in soft tissues and other spaces within the human body.

References

[1] R. J. Webster III, J. S. Kim, N. J. Cowan, G. S. Chirikjian, and A. M. Okamura, "Nonholonomic Modeling of Needle Steering," *Int J Robot. Res.*, vol. 25, no. 5-6, pp. 509–525, 2006.

[2] K. Reed, A. Majewicz, V. Kallem, R. Alterovitz, K. Goldberg, N. Cowan, and A. Okamura, "Robot-Assisted Needle Steering," *IEEE Robot. Autom. Mag.*, vol. 18, no. 4, pp. 35–46, 2011.

[3] S. Okazawa, R. Ebrahimi, J. Chuang, S. Salcudean, and R. Rohling, "Hand-Held Steerable Needle Device," *IEEE/ASME Trans. Mechatronics*, vol. 10, no. 3, pp. 285–296, 2005.

[4] N. Abolhassani, R. Patel, and M. Moallem, "Needle insertion into soft tissue: a survey." *Medical Engineering & Physics*, vol. 29, no. 4, pp. 413–31, 2007.

[5] D. C. Rucker, B. A. Jones, and R. J. Webster, "A Geometrically Exact Model for Externally Loaded Concentric-Tube Continuum Robots." *IEEE Trans. Robot.*, vol. 26, no. 5, pp. 769–780, 2010.

[6] P. E. Dupont, J. Lock, B. Itkowitz, and E. Butler, "Design and Control of Concentric-Tube Robots." *IEEE Trans. Robot.*, vol. 26, no. 2, pp. 209–225, 2010.

[7] J. Burgner, P. J. Swaney, D. C. Rucker, H. B. Gilbert, S. T. Nill, P. T. Russell, K. D. Weaver, and R. J. Webster III, "A bimanual teleoperated system for endonasal skull base surgery," in *IEEE/RSJ Int. Conf. on Intelligent Robots and Systems*, 2011, pp. 2517–2523.

[8] M. Mahvash and P. E. Dupont, "Stiffness Control of Surgical Continuum Manipulators," *IEEE Trans. Robot.*, vol. 27, no. 2, pp. 334–345, 2011.

[9] L. G. Torres and R. Alterovitz, "Motion planning for concentric tube robots using mechanics-based models," in *IEEE/RSJ Int. Conf. on Intelligent Robots and Systems*, 2011, pp. 5153–5159.

[10] J. Burgner, P. J. Swaney, T. L. Bruns, M. S. Clark, D. C. Rucker, and R. J. Webster III, "An Autoclavable Steerable Cannula Manual Deployment Device: Design and Accuracy Analysis," *ASME J Med. Devices*, vol. 6, no. 4, p. 041007, 2012.

[11] E. C. Burdette, D. C. Rucker, P. Prakash, C. J. Diederich, J. M. Croom, C. Clarke, P. Stolka, T. Juang, E. M. Boctor, and R. J. Webster III, "The ACUSITT ultrasonic ablator: the first steerable needle with an integrated interventional tool," in *SPIE Medical Imaging 2010: Ultrasonic Imaging, Tomography, and Therapy*, 2010.

[12] L. A. Lyons, R. J. Webster III, and R. Alterovitz, "Planning active cannula configurations through tubular anatomy," in *IEEE Int. Conf. on Robotics and Automation*, 2010, pp. 2082–2087.

[13] H. Choset and W. Henning, "A Follow-the-Leader Approach to Serpentine Robot Motion Planning," *Journal of Aerospace Engineering*, vol. 12, no. 2, pp. 65–73, 1999.

[14] K. Ikuta, M. Tsukamoto, and S. Hirose, "Shape memory alloy servo actuator system with electric resistance feedback and application for active endoscope," in *IEEE Int. Conf. on Robotics and Automation*. IEEE Comput. Soc. Press, 1988, pp. 427–430.

[15] A. Degani, H. Choset, B. Zubiate, T. Ota, and M. Zenati, "Highly articulated robotic probe for minimally invasive surgery." in *Int. Conf. of the IEEE Engineering in Medicine and Biology Society*, 2006, pp. 4157–4172.

[16] T. Anor, J. R. Madsen, and P. Dupont, "Algorithms for Design of Continuum Robots Using the Concentric Tubes Approach: A Neurosurgical Example." in *IEEE Int. Conf. on Robotics and Automation*, 2011, pp. 667–673.

[17] L. A. Lyons, R. J. Webster III, and R. Alterovitz, "Motion Planning for Active Cannulas," in *IEEE/RSJ Int. Conf. on Intelligent Robots and Systems (IROS)*, 2009, pp. 801–806.

[18] C. Bedell, J. Lock, A. Gosline, and P. E. Dupont, "Design Optimization of Concentric Tube Robots Based on Task and Anatomical Constraints." in *IEEE Int. Conf. on Robotics and Automation*, 2011, pp. 398–403.

[19] R. J. Webster III, J. M. Romano, and N. J. Cowan, "Mechanics of Precurved-Tube Continuum Robots," *IEEE Trans. Robot.*, vol. 25, no. 1, pp. 67–78, 2009.

[20] D. C. Rucker, R. J. Webster III, G. S. Chirikjian, and N. J. Cowan, "Equilibrium Conformations of Concentric-tube Continuum Robots," *Int J Robot. Res.*, vol. 29, no. 10, pp. 1263–1280, 2010.

[21] L. G. Torres, R. J. Webster III, and R. Alterovitz, "Task-Oriented Design of Concentric Tube Robots Using Mechanics-Based Models," in *IEEE/RSJ Int. Conf. on Intelligent Robots and Systems*, 2012, pp. 4449–4455.

[22] D. C. Rucker and R. J. Webster III, "Parsimonious evaluation of concentric-tube continuum robot equilibrium conformation." *IEEE Trans. Biomed. Eng.*, vol. 56, no. 9, pp. 2308–11, 2009.

[23] E. E. Greenblatt, K. I. Trovato, A. Popovic, and D. Stanton, "Interlocking Nested Cannula," 2011.

[24] J. Lock and P. E. Dupont, "Friction modeling in concentric tube robots," in *IEEE Int. Conf. on Robotics and Automation*, 2011, pp. 1139–1146.